AIMS Mathematics, 10(8): 19079–19105.
DOI: 10.3934/math.2025853
Received: 13 June 2025
Revised: 01 August 2025
Accepted: 11 August 2025
Published: 21 August 2025

https://www.aimspress.com/journal/Math

Research article

Fractional multivariable grey optimization model with interaction effects and its application

Shuangbing Guo, Huanyu Zhou*, Yuzhen Chen and Wenhao Gong

School of Mathematical Sciences, Henan Institute of Science and Technology, Xinxiang 453003, China

* **Correspondence:** Email: zhou.huanyu@stu.hist.edu.cn; Tel: +8615890371001.

Abstract: To further enhance the accuracy and stability of multivariate grey prediction models and expand their application scope, a fractional multivariate grey optimization model with interaction effects was proposed. Building upon traditional grey models, we optimized the background value parameters and introduced fractional-order accumulation to improve fitting accuracy. Additionally, the model fully incorporates interaction effects among driving factors and integrates linear and nonlinear correction terms to enhance adaptability. The developed model exhibits high flexibility, as it can degenerate into eight classical grey models through parameter adjustments. The genetic algorithm was employed to solve the optimal parameters for global optimization, and ablation experiments were conducted to verify the effectiveness of each component. Finally, the developed model was utilized in forecasting China's carbon dioxide emissions from energy consumption. It exhibits superior performance compared to existing models, excelling in both simulation accuracy and predictive capability. This confirms its strong adaptability and stability as an effective tool for predicting China's carbon dioxide emissions from energy consumption.

Keywords: multivariate grey prediction model; interaction effect; fractional-order accumulation; carbon dioxide emissions; the genetic algorithm
Mathematics Subject Classification: 62M10, 93E11, 90C30

1. Introduction

As global industrialization and urbanization accelerate, the world economy has grown rapidly in recent decades, leading to a sustained rise in energy demand. The energy supply is currently dominated

by fossil fuels [1]. The combustion of these fuels releases substantial quantities of carbon dioxide (CO_2), which is the primary source of greenhouse gas emissions. This aggravates environmental crises, such as global warming and the increasing occurrence of severe weather phenomena. To address this challenge, as the world's top CO_2 emitter, China proposed a "dual-carbon" strategy in 2020. In 2022, China further released the 14th Five-Year Plan for a Modern Energy System to accelerate the construction of a clean energy system centered on wind, solar, nuclear, and hydrogen energy. Currently, China leads the world in installed capacity of photovoltaic and wind power, has established a preliminary green hydrogen industry chain, and achieved breakthroughs in advanced nuclear power technologies. These transformative measures not only propel the energy structure toward a low-carbon transition but also contribute to global emission reduction through technology exports and production capacity cooperation. In this context, the scientific forecasting of CO_2 emissions from energy is of paramount importance for the strategic allocation of resources and for the harmonization of economic expansion with climate change mitigation efforts.

Given the growing threats posed by climate change, the scientific community and policymakers urgently require accurate predictions of future CO_2 emission trends to formulate scientifically rigorous emission reduction strategies. Globally, researchers utilize a variety of predictive methodologies to analyze CO_2 emissions. Hrithik et al. applied the ARIMA model to predict India's CO_2 emissions using data from 1990 to 2023 [2]. Duan et al. utilized the fixed-base energy consumption elasticity coefficient method to forecast energy consumption and CO_2 emissions [3]. Ghorbal et al. proposed a machine learning approach combining DPRNNs and NiOA for CO_2 emission prediction [4]. Moayedi et al. integrated multilayer perceptrons (MLP) with nature-inspired optimization algorithms for energy-related emission forecasting [5]. These studies significantly contribute to global carbon reduction efforts, yet they all rely heavily on extensive historical data to extract sufficient information. The grey system theory, proposed by Deng (1982), exhibits remarkable adaptability in small-sample and uncertain systems. It enables effective predictions and trend characterizations in such contexts [6]. Jiang et al. proposed a new discrete grey Bernoulli seasonal model to forecast monthly CO_2 emissions, which has better forecasting performance than SARIMA [7]. Qiao et al. employed the discrete grey model to predict CO_2 emissions across APEC economies, with their findings establishing an empirical basis for energy policy formulation [8]. China's 12th Five-Year Plan (2010) established CO_2 reduction as a key environmental policy objective, implementing a series of impactful measures. However, such policy interventions have substantially diminished the predictive value of historical data. Following the principle of new information priority, it is more reasonable to use recent data, though with a smaller sample size [9]. Compared with statistical and machine learning methods, the grey prediction method shows stronger advantages in dealing with uncertain systems with "small data and poor information".

The grey prediction model is a crucial part of grey system theory [10]. The model does not rely on large sample sizes and probability distribution assumptions from traditional statistics. This model is particularly valuable in domains with scarce data and unknown distribution patterns. Multivariate grey prediction models, which comprehensively account for the potential impacts of external conditions on system growth trends, not only demonstrate the robust functionality of grey prediction theory but have also been extensively utilized in energy [11,12], agriculture [13], and environmental studies [14,15]. With the advancement of grey system theory, scholars continue to refine these models to broaden their applicability. To enhance the performance of grey prediction models, researchers primarily focus on two dimensions: Parameter optimization and structural innovation.

Model parameters exert significant influences on the time response function and inverse accumulation generating operation. The optimization of parameters in grey prediction models primarily focuses on three aspects: Initial value optimization [16–18], background value optimization,

and accumulation order optimization. Deng proposed that first-order accumulation can reduce data randomness and reveal inherent patterns in originally featureless data [10]. However, traditional first-order accumulation shows limitations in broader applications. Therefore, scholars continue to study the method of accumulation. Wu et al. applied perturbation theory to prove that fractional-order accumulation fully incorporates the principle of new information priority, leading to significant improvements in model stability and prediction accuracy [19]. Kang et al. enhanced model fitting ability to complex time-response sequence data via dynamic adjustment of accumulation order [20]. Zeng et al. extended the fractional-order range from positive real numbers to all real numbers by expanding the Gamma function's domain [21]. Since the introduction of fractional-order accumulation, based on fractional-order accumulative generation, many fractional grey prediction models with better performance have been constructed. Chen et al. developed a conformable fractional-order accumulation framework integrated with multiple optimization techniques, achieving superior universality and stability [22]. Wang et al. put forward a Caputo fractional-order derivative-based structural adaptive nonlinear multivariate grey model [23]. For most grey prediction models, fractional-order accumulation can improve the accuracy of the model, which significantly advances the development of accumulation generation and the improvement of model stability and applicability.

The background value is also of great significance in enhancing the accuracy of the grey model. Zeng transformed background coefficients into dynamic parameters optimized via particle swarm optimization, significantly improving the grey model's predictive capability [24]. Huang et al. introduced fractional-order accumulation operators and background value optimization techniques into multivariate interval grey models, markedly enhancing forecasting accuracy for multivariate interval data [25]. Parameter optimization effectively mitigates errors from improper parameter selection, thereby improving both fitting and forecasting precision.

Scholars have continuously innovated the structure of grey models to expand their application domains and enhance performance. Xie et al. pioneered the grey discrete prediction model, laying the theoretical foundation for structural innovation [26]. Building on it, Ma et al. developed a discrete multivariate grey prediction model, enriching the framework of multivariable forecasting [27]. Ding et al. introduced virtual variable terms into the traditional grey model [GM(1,N)] to account for qualitative factors, thereby refining the model's structure [28]. Interaction effects generally exist in complex systems. For improved processing of small sample systems, Wang first integrated interaction terms into multivariate grey models, constructing an interactive grey prediction model [IEGM(1,N)]. Notably, this model reduces to the traditional GM(1,N) when interaction coefficients are zero [29]. Ding et al. built a multivariable model considering the interaction between driving factors and gave two derived models according to the magnitude of change. The three models can be transformed into each other [30]. Duan et al. integrated the logistic model of energy structure into system dynamics; the interaction between related factors and multiple major factors is described in the form of equations to improve applicability and stability [31]. Xia et al. proposed nonlinear correction functions featuring a dynamically adaptive structure with uncertainty, enabling automatic adjustment to data characteristics [32].

It is difficult for a single improved model to fully capture the changing law of data. To enhance adaptability and robustness, scholars have adopted multidimensional optimization strategies. Li et al. introduced fractional-order accumulation, linear correction terms, and grey action quantities into GM(1,N), establishing the FOBGM(1,N) model to reduce errors [33]. The proposed model integrates multiple optimization techniques, which not only accurately capture the complex system relationships but also significantly improve fitting accuracy. Zeng et al. improved prediction accuracy by incorporating dependent variable lag term, linear corrections, and random disturbance terms into the NMGM(1,N) model [34]. Si introduced the time-delay driving term, the interactive driving term, and

the power index, constructing the IEDGPM(1,N) model [35]. Li thoroughly considered the differential information and proposed a multivariate heterogeneous cumulative grey prediction model [HUGMC(1,N)] [36]. It can effectively enhance the model's stability, reduce the loss of differential information, and significantly improve both fitting and prediction performance.

The above research achievements have made outstanding contributions. However, practical systems often exhibit both complexity and stochasticity, presenting typical uncertainty characteristics of grey causality with white outcomes. To effectively expand the application boundaries and further enhance forecasting accuracy, this paper proposes the fractional multivariable grey optimization model with interaction effects [IEFOGM(r,N,λ,α)]. This model's parameter optimization is achieved through background value adjustment and fractional-order accumulation operations. Considering the interaction between the drivers, linear and nonlinear correction terms are added to improve model performance. The IEFOGM(r,N,λ,α) model builds upon the FMGM(1,N) by incorporating interaction terms to capture the interplay among relevant factors. Additionally, it employs a dynamic background value, endowing the model with higher fitting precision and enhanced adaptability. The NSGM(1,N) replaces the shadow equation with a difference model to ensure homology between parameter estimation and application. The IEFOGM(r,N,λ,α) offers two critical improvements. First, the IEFOGM model is rooted in the NSGM(1,N) model. Compared with the IEGM(1,N) model, the IEFOGM reduces errors caused by the lack of homology between parameter estimation and parameter application. Second, by integrating fractional-order accumulation, linear correction term, and nonlinear correction term, the IEFOGM(r,N,λ,α) achieves superior adaptability and stability in complex modeling contexts. Ultimately, the model is applied to the prediction of carbon dioxide emissions from energy consumption, which is of great significance for climate change research and the construction of carbon emission reduction policies.

2. Methodology

2.1. The NSGM(1,N) model

Definition 1. [37] Let the system characteristic data sequence be $X_1^{(0)} = (x_1^{(0)}(1), x_1^{(0)}(2), \cdots, x_1^{(0)}(n))$, and the relevant factor sequence be $X_j^{(0)} = (x_j^{(0)}(1), x_j^{(0)}(2), \cdots, x_j^{(0)}(n)), j = 2, 3, \cdots, N$. $X_j^{(1)}$ is the first-order accumulation generating sequence of $X_j^{(0)}$, where

$$x_j^{(1)}(k) = \sum_{j=1}^{k} x_j^{(0)}(k), k = 1, 2, \cdots, n. \tag{1}$$

$Z_1^{(1)}$ is the adjacent mean generated sequence of $X_1^{(1)}$, where

$$z_1^{(1)}(k) = \frac{1}{2}\left(\hat{x}_1^{(1)}(k) + \hat{x}_1^{(1)}(k-1)\right), k = 2, 3, \cdots, n. \tag{2}$$

The following equation

$$x_1^{(0)}(k) + az_1^{(1)}(k) = \sum_{j=2}^{N} b_j x_j^{(1)}(k) + h_1(k-1) + h_2 \tag{3}$$

is called the novel structural grey prediction model, abbreviated as the NSGM(1,N) model. In this formula, a represents the system development coefficient, b_j denotes the driving coefficient, and $h_1(k-1)$ and h_2 are termed the linear correction term and grey action quantity.

Theorem 1. Let $X_1^{(0)}$, $X_j^{(0)}$, $Z_1^{(1)}$ be the same as Definition 1, then the parameter sequence $\hat{p}=\left[b_2,\cdots,b_N,b_{N+1},a,h_1,h_2\right]^T$ in the NSGM(1,N) model is expressed as

$$\hat{p}=(B^TB)^{-1}B^TY, \tag{4}$$

where

$$B=\begin{bmatrix} x_2^{(1)}(2) & x_3^{(1)}(2) & \cdots & x_N^{(1)}(2) & -z_1^{(1)}(2) & 1 & 1 \\ x_2^{(1)}(3) & x_3^{(1)}(3) & \cdots & x_N^{(1)}(3) & -z_1^{(1)}(3) & 2 & 1 \\ \vdots & \vdots & \ddots & \vdots & \vdots & \vdots & \vdots \\ x_2^{(1)}(n) & x_3^{(1)}(n) & \cdots & x_N^{(1)}(n) & -z_1^{(1)}(n) & n-1 & 1 \end{bmatrix}_{(n-1)\times(N+2)}, \quad Y=\begin{bmatrix} x_1^{(0)}(2) \\ x_1^{(0)}(3) \\ \vdots \\ x_1^{(0)}(n) \end{bmatrix}.$$

Definition 2. The NSGM(1,N) model is described in Definition 1, and the parameter column $\hat{p}=\left[b_2,\cdots,b_N,b_{N+1},a,h_1,h_2\right]^T$ is described in Theorem 1,

$$\hat{x}_1^{(0)}(k)=\sum_{i=2}^{N}b_ix_i^{(1)}(k)-az_1^{(1)}(k)+h_1(k-1)+h_2. \tag{5}$$

Equation (5) is the difference model of NSGM(1,N) model.

Theorem 2. The difference model of NSGM(1,N) is described in Definition 2; let $\hat{x}_1^{(1)}(1)=x_1^{(0)}(1)$, and the time response sequence of the NSGM(1,N) model is

$$\hat{x}_1^{(1)}(k)=\sum_{\nu=1}^{k-1}[\mu_1\sum_{j=2}^{N}\mu_2^{\nu-1}b_jx_j^{(1)}(k-\nu+1)]+\mu_2^{k-1}\hat{x}_1^{(1)}(1)+\sum_{s=0}^{k-2}\mu_2^s[(k-s)\mu_3+\mu_4], \tag{6}$$

where $\mu_1=\dfrac{1}{1+0.5a}$, $\mu_2=\dfrac{1-0.5a}{1+0.5a}$, $\mu_3=\dfrac{h_1}{1+0.5a}$, $\mu_4=\dfrac{h_2-h_1}{1+0.5a}$.

Its cumulative reduction formula is

$$\hat{x}_1^{(0)}\left(k\right)=\hat{x}_1^{(1)}\left(k\right)-\hat{x}_1^{(1)}\left(k-1\right),k=2,3,...,n. \tag{7}$$

The NSGM(1,N) model derives the time response sequences using the difference model, which is entirely derived from the equivalent transformation of the NSGM(1,N) model. This ensures homology between parameter estimation and application, effectively reducing model errors [37].

2.2. The construction of the IEFOGM(r,N,λ,α) model

Definition 3. [21] Let $r\in R$, $X_1^{(0)}$, $X_i^{(0)}$ as defined by definition 1, where $X_i^{(r)}=(x_i^{(r)}(1),x_i^{(r)}(2),\cdots,x_i^{(r)}(n))$ is the r-order accumulation generating sequence of $X_i^{(0)}$, denoted as r-AGO, where

$$x_i^{(r)}(k)=\sum_{j=1}^{k}\frac{\Gamma(r+k-j)}{\Gamma(k-j+1)\Gamma(r)}x_i^{(0)}(j),k=1,2,\cdots,n. \tag{8}$$

The Γ in the above equation represents the gamma function.

On the contrary, $X_i^{(-r)} = (x_i^{(-r)}(1), x_i^{(-r)}(2), \cdots, x_i^{(-r)}(n))$ is the r-order inverse accumulation generating sequence of $X_i^{(0)}$, denoted as r-IAGO, where

$$X_i^{(-r)}(k) = \sum_{j=0}^{k-1} (-1)^j \frac{\Gamma(r+k-j)}{\Gamma(r-j+1)\Gamma(r)} x_i^{(0)}(k-j), k = 1, 2, \cdots, n . \tag{9}$$

Definition 4. Let the system behavior sequence be $X_1^{(0)} = (x_1^{(0)}(1), x_i^{(0)}(2), \cdots, x_1^{(0)}(n))$, the sequence of relevant factors is $X_i^{(0)}, i = 2, \cdots, N$, $X_i^{(r)}$ is the r-AGO of $X_i^{(0)}$, and $Z_1^{(r)}$ is the dynamic background value generation sequence, where

$$z_1^{(r)}(k) = \lambda \hat{x}_1^{(r)}(k) + (1-\lambda)\hat{x}_1^{(r)}(k-1), (0 \le \lambda \le 1). \tag{10}$$

The following equation

$$x_1^{(r-1)}(k) + a z_1^{(r)}(k) = \sum_{i=2}^{N} b_i x_i^{(r)}(k) + \sum_{p=2}^{N} \sum_{q=p+1}^{N} b_{pq} x_p^{(r)}(k) x_q^{(r)}(k) + h_1 k^{\alpha} + h_2 k + h_3 \tag{11}$$

is called the fractional multivariable grey optimization model with interaction effects, abbreviated as IEFOGM(r,N,λ,α).

Here, a is the coefficient of development, b_i is the driving coefficient, $b_i x_i^{(r)}(k)$ is the driving term, b_{pq} is the interactive driving coefficient, $b_{pq} x_p^{(r)}(k) x_q^{(r)}(k)$ is the interactive driver, $h_1 k^{\alpha}$ is the nonlinear correction term, $h_2 k$ is the linear correction term, and h_3 is the grey action. Parameter r represents the fractional-order accumulation order, α is the nonlinear term exponent, and λ denotes the coefficient of the dynamic background value.

Theorem 3. Let the sequence $X_i^{(0)}, X_i^{(r)}, Z_1^{(r)}$ be defined as in Definition 4. Then, the parameter sequence $\hat{p} = \left[b_2, b_3, \cdots, b_N, b_{23}, \cdots, b_{(N-1)N}, a, h_1, h_2, h_3\right]^T$ in the IEFOGM(r,N,λ,α) model is expressed as

(1) when $n = N + C_{N-1}^2 + 4$, $\hat{p} = B^{-1}Y$;

(2) when $n > N + C_{N-1}^2 + 4$, $\hat{p} = (B^T B)^{-1} B^T Y$;

(3) when $n < N + C_{N-1}^2 + 4$, $\hat{p} = B^T (B^T B)^{-1} Y$;

where

$$B = \begin{bmatrix} x_2^{(r)}(2) & x_3^{(r)}(2) & \cdots & x_N^{(r)}(2) & x_2^{(r)}(2)x_3^{(r)}(2) & \cdots x_{N-1}^{(r)}(2)x_N^{(r)}(2) & -z_1^{(r)}(2) & 2^{\alpha} & 2 & 1 \\ x_2^{(r)}(3) & x_3^{(r)}(3) & \cdots & x_N^{(r)}(3) & x_2^{(r)}(3)x_3^{(r)}(3) & \cdots x_{N-1}^{(r)}(3)x_N^{(r)}(3) & -z_1^{(r)}(3) & 3^{\alpha} & 3 & 1 \\ \vdots & \vdots & \ddots & \vdots & \vdots & \ddots & \vdots & \vdots & \vdots & \vdots \\ x_2^{(r)}(n) & x_3^{(r)}(n) & \cdots & x_N^{(r)}(n) & x_2^{(r)}(n)x_3^{(r)}(n) & \cdots x_{N-1}^{(r)}(n)x_N^{(r)}(n) & -z_1^{(r)}(n) & n^{\alpha} & n & 1 \end{bmatrix}_{(n-1)\times\left(N+3+C_{N-1}^2\right)}$$

$$Y = \begin{bmatrix} x_1^{(r)}(2) - x_1^{(r-1)}(1) \\ x_1^{(r)}(3) - x_1^{(r-1)}(2) \\ \vdots \\ x_1^{(r)}(n) - x_1^{(r-1)}(n-1) \end{bmatrix}.$$

The proof process is similar to that in [13] and will be omitted here.

Definition 5. The IEFOGM(r,N,λ,α) model was described in Definition 4, with parameter sequence $\hat{p}$ as shown in Theorem 3; then the difference model of IEFOGM(r,N,λ,α) is

$$\hat{x}_1^{(r-1)}(k)=\sum_{i=2}^{N}b_i x_i^{(r)}(k)+\sum_{p=2}^{N}\sum_{q=p+1}^{N}b_{pq}x_p^{(r)}(k)x_q^{(r)}(k)-az_1^{(r)}(k)+h_1k^{\alpha}+h_2k+h_3, \tag{12}$$

where

$$\hat{x}_1^{(r-1)}(k)=\hat{x}_1^{(r)}(k)-\hat{x}_1^{(r)}(k-1). \tag{13}$$

Theorem 4. The IEFOGM(r,N,λ,α) model and its parameter set $\hat{p}$ are described in Definition 4 and Theorem 3. Let $\hat{x}_1^{(r)}(1)=x_1^{(0)}(1)$, when $k=2,3,\cdots,n$.

(1) The time response formula of the IEFOGM(r, N, λ, α) model is

$$\begin{aligned}\hat{x}_1^{(r)}(k)=&\sum_{\nu=1}^{k-1}\left\{\mu_1\mu_2^{\nu-1}\left[\sum_{i=2}^{N}b_i x_i^{(r)}(k-\nu+1)+\sum_{p=2}^{N}\sum_{q=p+1}^{N}b_{pq}x_p^{(r)}(k-\nu+1)x_q^{(r)}(k-\nu+1)\right]\right\}\\&+\mu_2^{k-1}\hat{x}_1^{(1)}(1)+\sum_{u=2}^{k}\mu_3\mu_2^{k-u}u^{\alpha}+\sum_{s=0}^{k-2}\mu_2^{s}\left[(k-s)\mu_4+\mu_5\right],\end{aligned} \tag{14}$$

where $\mu_1=\dfrac{1}{1+a\lambda}$, $\mu_2=\dfrac{1-a(1-\lambda)}{1+a\lambda}$, $\mu_3=\dfrac{h_1}{1+a\lambda}$, $\mu_4=\dfrac{h_2}{1+a\lambda}$, $\mu_5=\dfrac{h_3}{1+a\lambda}$.

(2) The inverse accumulated formula of the IEFOGM(r, N, λ, α) model is

$$\hat{x}_1^{(0)}(k)=(\hat{x}_1^{(r)})^{(-r)}(k)=\sum_{j=0}^{k}(-1)^i\frac{\Gamma(r+1)}{\Gamma(j+1)\Gamma(r-j+1)}\hat{x}_1^{(r)}(k-j). \tag{15}$$

Proof. (1) When $k=2,3,\cdots,n$, by Definition 5, we obtain

$$\hat{x}_1^{(r-1)}(k)=\sum_{i=2}^{N}b_i x_i^{(r)}(k)+\sum_{p=2}^{N}\sum_{q=p+1}^{N}b_{pq}x_p^{(r)}(k)x_q^{(r)}(k)-az_1^{(r)}(k)+h_1k^{\alpha}+h_2k+h_3. \tag{16}$$

$$z_1^{(r)}(k)=\lambda\hat{x}_1^{(r)}(k)+(1-\lambda)\hat{x}_1^{(r)}(k-1),k=2,3,\cdots,n\ . \tag{17}$$

By substituting Eqs (13) and (17) into Eq (16), we obtain

$$\begin{aligned}\hat{x}_1^{(r)}(k)-\hat{x}_1^{(r)}(k-1)=&\sum_{i=2}^{N}b_i x_i^{(r)}(k)+\sum_{p=2}^{N}\sum_{q=p+1}^{N}b_{pq}x_p^{(r)}(k)x_q^{(r)}(k)-\\&a\left[\lambda\hat{x}_1^{(r)}(k)+(1-\lambda)\hat{x}_1^{(r)}(k-1)\right]+h_1k^{\alpha}+h_2k+h_3.\end{aligned} \tag{18}$$

Rearranging Eq (18) yields

$$\begin{aligned}\hat{x}_1^{(r)}(k)=&\frac{1}{1+a\lambda}\left[\sum_{i=2}^{N}b_i x_i^{(r)}(k)+\sum_{p=2}^{N}\sum_{q=p+1}^{N}b_{pq}x_p^{(r)}(k)x_q^{(r)}(k)\right]\\&+\frac{1-a(1-\lambda)}{1+a\lambda}\hat{x}_1^{(r)}(k-1)+\frac{h_1k^{\alpha}}{1+a\lambda}+\frac{h_2k}{1+a\lambda}+\frac{h_3}{1+a\lambda}.\end{aligned} \tag{19}$$

Let $\mu_1=\dfrac{1}{1+a\lambda}$, $\mu_2=\dfrac{1-a(1-\lambda)}{1+a\lambda}$, $\mu_3=\dfrac{h_1}{1+a\lambda}$, $\mu_4=\dfrac{h_2}{1+a\lambda}$, $\mu_5=\dfrac{h_3}{1+a\lambda}$.

Then Eq (19) can be transformed into

$$\begin{aligned}\hat{x}_1^{(r)}(k) &= \mu_1\left[\sum_{i=2}^{N} b_i x_i^{(r)}(k) + \sum_{p=2}^{N}\sum_{q=p+1}^{N} b_{pq} x_p{}^{(r)}(k) x_q{}^{(r)}(k)\right] \\ &\quad + \mu_2 \hat{x}_1^{(r)}(k-1) + \mu_3 k^{\alpha} + \mu_4 k + \mu_5.\end{aligned} \tag{20}$$

As shown in Eq (20), when $k = 2$,

$$\hat{x}_1^{(r)}(2) = \mu_1\left[\sum_{i=2}^{N} b_i x_i^{(r)}(2) + \sum_{p=2}^{N}\sum_{q=p+1}^{N} b_{pq} x_p{}^{(r)}(2) x_q{}^{(r)}(2)\right] + \mu_2 x_1^{(0)}(1) + \mu_3 2^{\alpha} + 2\mu_4 + \mu_5. \tag{21}$$

When $k = 3$,

$$\hat{x}_1^{(r)}(3) = \mu_1[\sum_{i=2}^{N} b_i x_i^{(r)}(3) + \sum_{p=2}^{N}\sum_{q=p+1}^{N} b_{pq} x_p{}^{(r)}(3) x_q{}^{(r)}(3)] + \mu_2 \hat{x}_1^{(r)}(2) + \mu_3 3^{\alpha} + 3\mu_4 + \mu_5. \tag{22}$$

Substitution of Eq (21) into Eq (22) leads to

$$\begin{aligned}\hat{x}_1^{(r)}(3) &= \mu_1\left[\sum_{i=2}^{N} b_i x_i^{(r)}(3) + \sum_{p=2}^{N}\sum_{q=p+1}^{N} b_{pq} x_p{}^{(r)}(3) x_q{}^{(r)}(3)\right] \\ &\quad + \mu_1\mu_2\left[\sum_{i=2}^{N} b_i x_i^{(r)}(2) + \sum_{p=2}^{N}\sum_{q=p+1}^{N} b_{pq} x_p{}^{(r)}(2) x_q{}^{(r)}(2)\right] \\ &\quad + \mu_2^2 x_1^{(0)}(1) + \mu_2\mu_3 2^{\alpha} + \mu_3 3^{\alpha} + 2\mu_2\mu_4 + \mu_2\mu_5 + 3\mu_4 + \mu_5 \\ &= \sum_{\nu=1}^{2}\left\{\mu_1\mu_2^{\nu-1}\left[\sum_{i=2}^{N} b_i x_i^{(r)}(4-\nu) + \sum_{p=2}^{N}\sum_{q=p+1}^{N} b_{pq} x_p^{(r)}(4-\nu) x_q^{(r)}(4-\nu)\right]\right\} \\ &\quad + \mu_2^2 x_1^{(0)}(1) + \sum_{u=2}^{3}\mu_3\mu_2^{3-u}u^{\alpha} + \sum_{s=0}^{1}\mu_2^{s}\left[(3-s)\mu_4 + \mu_5\right].\end{aligned} \tag{23}$$

When $k = 4$,

$$\begin{aligned}\hat{x}_1^{(r)}(4) &= \mu_1\left[\sum_{i=2}^{N} b_i x_i^{(r)}(4) + \sum_{p=2}^{N}\sum_{q=p+1}^{N} b_{pq} x_p{}^{(r)}(4) x_q{}^{(r)}(4)\right] \\ &\quad + \mu_2 \hat{x}_1^{(r)}(3) + \mu_3 4^{\alpha} + 4\mu_4 + \mu_5.\end{aligned} \tag{24}$$

Combining Eq (23) with Eq (24) leads to

$$\begin{aligned}\hat{x}_1^{(r)}(4) &= \mu_1\sum_{i=2}^{N} b_i x_i^{(r)}(4) + \mu_1\sum_{p=2}^{N}\sum_{q=p+1}^{N} b_{pq}x_p{}^{(r)}(4)x_q{}^{(r)}(4) + \mu_1\mu_2\sum_{i=2}^{N} b_i x_i^{(r)}(3)\\ &+ \mu_1\mu_2\sum_{p=2}^{N}\sum_{q=p+1}^{N} b_{pq}x_p{}^{(r)}(3)x_q{}^{(r)}(3) + \mu_1\mu_2^2\sum_{i=2}^{N} b_i x_i^{(r)}(2)\\ &+ \mu_1\mu_2^2\sum_{p=2}^{N}\sum_{q=p+1}^{N} b_{pq}x_p{}^{(r)}(2)x_q{}^{(r)}(2) + \mu_2^3 x_1^{(0)}(1) + \mu_2^2\mu_3 2^{\alpha} + 2\mu_2^2\mu_4\\ &+ \mu_2^2\mu_5 + \mu_2\mu_3 3^{\alpha} + 3\mu_2\mu_4 + \mu_2\mu_5 + \mu_3 4^{\alpha} + 4\mu_4 + \mu_5\\ &= \sum_{\nu=1}^{3}\left\{\mu_1\mu_2^{\nu-1}\left[\sum_{i=2}^{N} b_i x_i^{(r)}(5-\nu) + \sum_{p=2}^{N}\sum_{q=p+1}^{N} b_{pq}x_p^{(r)}(5-\nu)x_q^{(r)}(5-\nu)\right]\right\}\\ &+ \mu_2^3 x_1^{(0)}(1) + \sum_{u=2}^{4}\mu_3\mu_2^{4-u}u^{\alpha} + \sum_{s=0}^{2}\mu_2^s\left[(4-s)\mu_4 + \mu_5\right].\end{aligned} \tag{25}$$

When $k = t$,

$$\begin{aligned}\hat{x}_1^{(r)}(t) &= \mu_1\left[\sum_{i=2}^{N} b_i x_i^{(r)}(t) + \sum_{p=2}^{N}\sum_{q=p+1}^{N} b_{pq}x_p^{(r)}(t)x_q^{(r)}(t)\right] + \mu_1\mu_2\left[\sum_{i=2}^{N} b_i x_i^{(r)}(t-1)\right.\\ &\left.+\sum_{p=2}^{N}\sum_{q=p+1}^{N} b_{pq}x_p^{(r)}(t-1)x_q^{(r)}(t-1)\right] + \cdots + \mu_1\mu_2{}^{t-2}\sum_{i=2}^{N} b_i x_i^{(r)}(2)\\ &+ \mu_1\mu_2{}^{t-2}\sum_{p=2}^{N}\sum_{q=p+1}^{N} b_{pq}x_p^{(r)}(2)x_q^{(r)}(2) + \mu_2^{t-1}x_1^{(0)}(1) + \mu_2^{t-2}\mu_3 2^{\alpha} + 2\mu_2^{t-2}\mu_4\\ &+ \mu_2^{t-2}\mu_5 + \mu_2{}^{t-3}\mu_3 3^{\alpha} + 3\mu_2{}^{t-3}\mu_4 + \mu_2{}^{t-3}\mu_5 + \cdots + \mu_3 t^{\alpha} + t\mu_4 + \mu_5.\end{aligned} \tag{26}$$

It comes down to

$$\begin{aligned}\hat{x}_1^{(r)}(k) &= \sum_{\nu=1}^{k-1}\left\{\mu_1\mu_2^{\nu-1}\left[\sum_{i=2}^{N} b_i x_i^{(r)}(k-\nu+1) + \sum_{p=2}^{N}\sum_{q=p+1}^{N} b_{pq}x_p^{(r)}(k-\nu+1)x_q^{(r)}(k-\nu+1)\right]\right\}\\ &+ \mu_2^{k-1}x_1^{(0)}(1) + \sum_{u=2}^{k}\mu_3\mu_2^{k-u}u^{\alpha} + \sum_{s=0}^{k-2}\mu_2^s\left[(k-s)\mu_4 + \mu_5\right],\end{aligned} \tag{27}$$

where $k = 2,3,\cdots,n$, and part (1) is proved.

(2) According to the literature [38],

$$X_i^{(0)} = (X_i^{(r)})^{(-r)} = (X_i^{(-r)})^{(r)}. \tag{28}$$

$$X_i^{(-r)}(k) = \sum_{j=0}^{k-1}(-1)^j\frac{\Gamma(r+k-j)}{\Gamma(r-j+1)\Gamma(r)}x_i^{(0)}(k-j). \tag{29}$$

By substituting Eq (28) into Eq (29), the cumulative reduction formula is

$$\hat{x}_1^{(0)}(k) = (\hat{x}_1^{(r)})^{(-r)}(k) = \sum_{j=0}^{k}(-1)^i\frac{\Gamma(r+1)}{\Gamma(j+1)\Gamma(r-j+1)}\hat{x}_1^{(r)}(k-j), \tag{30}$$

and part (2) is proved.

2.3. Parameter optimization

We discussed the construction of the IEFOGM(r,N,λ,α) model in the previous section. However, three parameters in the model, α, r, λ, remain unknown. To identify the optimal parameter, in this part, we formulate a nonlinear optimization problem aimed at the MAPE minimization for the proposed model. A smaller MAPE value indicates better model performance. The model's parameters are optimized through a genetic algorithm, with the objective of MAPE minimization. The specific objective function and constraints are detailed below.

$$\min MAPE(\alpha, r, \lambda) = \frac{1}{n-1}\sum_{k=2}^{n}\frac{\left|\hat{x}^{(0)}(k) - x^{(0)}(k)\right|}{x^{(0)}(k)}. \tag{31}$$

$$s.t.\begin{cases} \hat{x}_1^{(r)}(k) = \sum\limits_{\nu=1}^{k-1}\left\{\mu_1\mu_2^{\nu-1}\left[\sum\limits_{i=2}^{N} b_i x_i^{(r)}(k-\nu+1) + \sum\limits_{p=2}^{N}\sum\limits_{q=p+1}^{N} b_{pq}x_p^{(r)}(k-\nu+1)x_q^{(r)}(k-\nu+1)\right]\right\} \\ \qquad\qquad + \mu_2^{k-1}\hat{x}_1^{(1)}(1) + \sum\limits_{u=2}^{k}\mu_3\mu_2^{k-u}u^{\alpha} + \sum\limits_{s=0}^{k-2}\mu_2^{s}\left[(k-s)\mu_4 + \mu_5\right], \\ \hat{x}_1^{(0)}(k) = (\hat{x}_1^{(r)})^{(-r)}(k) = \sum\limits_{j=0}^{k}(-1)^i\dfrac{\Gamma(r+1)}{\Gamma(j+1)\Gamma(r-j+1)}\hat{x}_1^{(r)}(k-j), \\ \hat{p} = \left[b_2, b_3, \cdots, b_N, b_{23}, \cdots, b_{(N-1)N}, a, h_1, h_2, h_3\right]^T = \left(B^TB\right)^{-1}B^TY. \end{cases}$$

2.4. Properties of the IEFOGM(r,N,λ,α) model

Through appropriate parameter selection, the flexible IEFOGM(r,N,λ,α) model can be reduced to various conventional grey prediction models. When different parameter values are assigned, they correspond to different grey models, as specified in Table 1.

Property 1: When $b_i = 0, b_{pq} = 0, r = 1, \lambda = 0.5, \alpha = 0, h_1 + h_3 \neq 0, h_2 = 0$, the IEFOGM(r,N,λ,α) model can be transformed into the GM(1,1) model.

Property 2: When $b_i = 0, b_{pq} = 0, r = 1, \lambda = 0.5, \alpha = 1, h_1 = 0, h_2 \neq 0, h_3 = 0$, the IEFOGM(r,N,λ,α) model can be transformed into the NGM(1,1,k) model.

Property 3: When $N \geq 2, b_{pq} = 0, r = 1, \lambda = 0.5, h_1 = 0, h_2 \neq 0, h_3 \neq 0$, the IEFOGM(r,N,λ,α) model can be transformed into the TDGN(1,1) model.

Property 4: When $N \geq 2, b_{pq} = 0, r = 1, \lambda = 0.5, h_1 = 0, h_2 = 0, h_3 = 0$, the IEFOGM(r,N,λ,α) model can be transformed into the GM(1,N) model.

Property 5: When $N \geq 2, b_{pq} = 0, r = 1, \lambda = 0.5, \alpha = 0, h_1 + h_3 \neq 0, h_2 = 0$, the IEFOGM(r,N,λ,α) model can be transformed into the DGM(1,N) model.

Property 6: When $N \geq 2, b_{pq} = 0, r = 1, \lambda = 0.5, \alpha = 0, h_1 + h_3 \neq 0, h_2 \neq 0$, the IEFOGM(r,N,λ,α) model can be transformed into the NSGM(1,N) model.

Property 7: When $N \geq 2, b_{pq} = 0, \lambda = 0.5$, the IEFOGM(r,N,λ,α) model can be transformed into the FMGM(1,N) model.

Property 8: When $N \geq 2, \lambda = 0.5, \alpha = 0, h_1 + h_3 \neq 0, h_2 = 0$, the IEFOGM(r,N,λ,α) model can be transformed into the IEGM(1,N) model.

Table 1. Conventional grey models.

Number	Model	Basic form of the model
1	GM(1,1)	$x^{(0)}(k)+az^{(1)}(k)=b$ [10]
2	NGM(1,1,k)	$x^{(0)}(k)+az^{(1)}(k)=kb$ [39]
3	TDGM(1,1)	$x^{(0)}(k)+az^{(1)}(k)=kb+c$ [37]
4	GM(1,N)	$x_1^{(0)}(k)+az_1^{(1)}(k)=\sum_{i=2}^{N}b_i x_i^{(1)}(k)$ [10]
5	DGM(1,N)	$x_1^{(1)}(k)+\beta_1 x_1^{(1)}(k-1)=\sum_{i=2}^{N}\beta_i x_i^{(1)}(k)+\beta_{N+1}$ [26]
6	NSGM(1,N)	$x_1^{(0)}(k)+az_1^{(1)}(k)=\sum_{i=2}^{N}b_i x_i^{(1)}(k)+h_1(k-1)+h_2$ [37]
7	FMGM(1,N)	$x_1^{(r-1)}(k)+az_1^{(r)}(k)=\sum_{i=2}^{N}b_i x_i^{(r)}(k)+h_1k^{\alpha}+h_2k+h_3$ [40]
8	IEGM(1,N)	$x_1^{(0)}(k)+az_1^{(1)}(k)=\sum_{p,q\in i,p\neq q}b_{pq}x_p^{(1)}(k)x_q^{(1)}(k)+b_1+\sum_{i=2}^{N}b_i x_i^{(1)}(k)$ [41]

2.5. Construction steps of the IEFOGM(r,N,λ,α) model

Based on the aforementioned studies, the detailed modeling procedures for constructing the IEFOGM(r,N,λ,α) model are as follows. The corresponding modeling flowchart is illustrated in Figure 1.

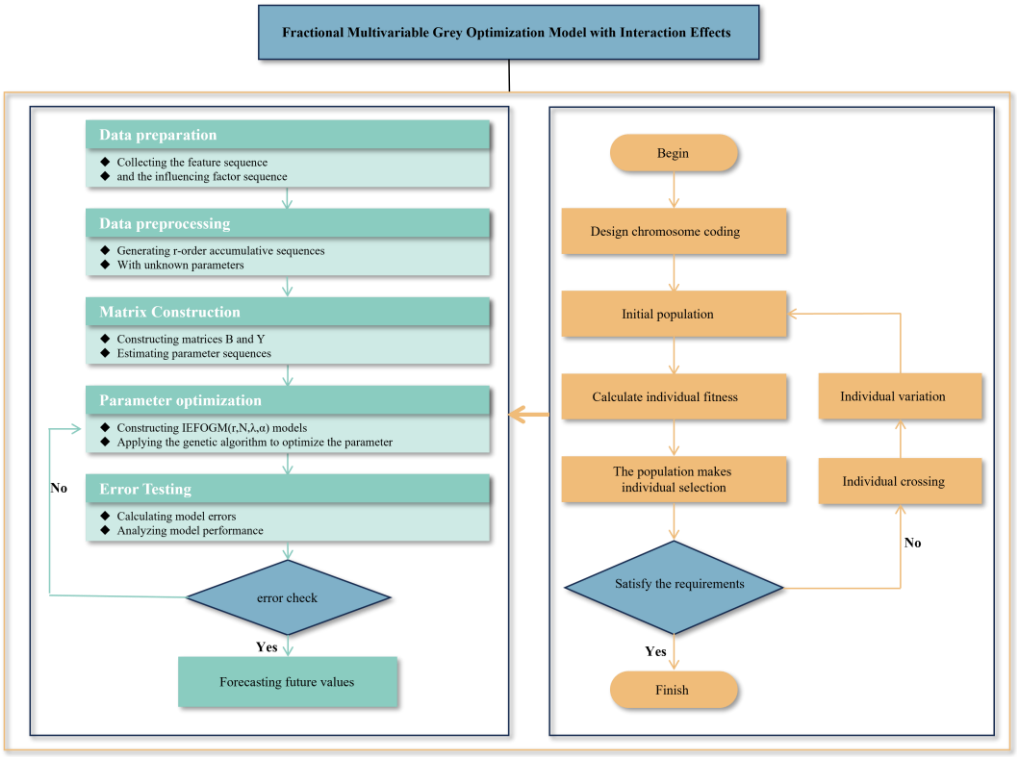

Figure 1. IEFOGM(r,N,λ,α) model flowchart.

Step 1. Data preparation: Collect raw data; first, determine the system's characteristic sequence and identify relevant factors through correlation analysis, and then partition the training set and testing set

based on actual conditions.

Step 2. Data preprocessing: Generate the r-order accumulated sequence of unknown order.

Step 3. Matrix construction: Based on Theorem 3, construct matrices B and Y containing the unknown hyperparameters α, r, λ, then estimate the parameter sequence

$$\hat{p} = \left[b_2, b_3, \cdots, b_N, b_{23}, \cdots, b_{(N-1)N}, a, h_1, h_2, h_3 \right]^T .$$

Step 4. Parameter optimization: Employ the genetic algorithms to search for the optimal parameters, and then determine the optimal parameter set.

Step 5. Model construction: According to Theorem 4, the time response sequence and final recovery sequence of the IEFOGM(r,N,λ,α) model are derived.

Step 6. Error testing: Calculate the error of the model for a comprehensive evaluation and analyze model performance.

Step 7. Predict future values and formulate corresponding strategies. The IEFOGM(r,N,λ,α) model is utilized to predict future values, followed by an analysis of the validity of the prediction results. Finally, the corresponding strategy and recommendations are proposed based on the predicted future values.

3. Model validation

3.1. Testing method

To validate the modeling efficacy of the IEFOGM(r,N,λ,α) model, this paper adopts the average percentage error (APE), mean absolute percentage error (MAPE), mean absolute error (MAE), and root mean square error (RMSE) as evaluation indicators.

$$APE = \frac{\left| \hat{x}^{(0)}(k) - x^{(0)}(k) \right|}{x^{(0)}(k)} . \tag{32}$$

$$MAPE = \frac{1}{n-1} \sum_{k=2}^{n} \frac{\left| \hat{x}^{(0)}(k) - x^{(0)}(k) \right|}{x^{(0)}(k)} . \tag{33}$$

$$MAE = \frac{1}{n-1} \sum_{k=2}^{n} \left| \hat{x}^{(0)}(k) - x^{(0)}(k) \right| . \tag{34}$$

$$RMSE = \sqrt{\frac{1}{n-1} \sum_{k=2}^{n} \left(\hat{x}^{(0)}(k) - x^{(0)}(k) \right)^2} . \tag{35}$$

3.2. Performance verification

To verify the effectiveness of the IEFOGM(r,N,λ,α) model, it is validated through practical case analysis and compared with other models.

Case 1. Forecast of China's nuclear power consumption.

To achieve sustainable development goals, China is actively promoting energy structure adjustment and vigorously developing clean energy sources. Nuclear power, as a highly efficient and

low-carbon energy form characterized by stability and reliability, has become a critical component of China's energy strategy. Forecasting China's nuclear power consumption not only holds significant implications for energy structure optimization and environmental protection but also provides important reference for policy making, investment decisions, and technological innovation. The nuclear power consumption data from literature [40] were selected for simulation and forecasting. China's nuclear power consumption and its related factors are presented in Table 2. The IEFOGM, FMGM, NSGM, GM(1,1), and ARIMA models were employed for fitting and prediction, with the results presented in Table 3. Figure 2 presents the comparative results between the fitted values of all candidate models and the original data sequence.

Table 2. Nuclear energy consumption in China and its related factors.

Years	Nuclear power consumption (Mtoe)	Population (10k people)	GDP (100 million yuan）
2010	17.12	134,091	412,119.3
2011	19.85	134,916	487,940.2
2012	22.24	135,922	538,580
2013	25.07	136,726	592,963.2
2014	29.78	127,646	643,563.1
2015	38.08	138,326	688,858.2
2016	47.09	139,232	746,395.1
2017	54.48	140,011	832,035.9
2018	64.40	140,541	919,281.1
2019	75.84	141,008	986,515.2
2020	79.35	141,212	1013,567
2021	87.98	141,260	1143,669.7
2022	89.81	141,175	1210,207.2

Table 3. Comparison of fitting accuracy of different models for nuclear power consumption in China.

	Years	Raw data	IEFOGM (r,N,λ,α)	FMGM (1,N,α)	FMGM (1,N)	NSGM (1,N)	GM(1,1)	ARIMA
Training set	2010	17.12	17.12	17.12	17.12	17.12	17.12	47.24
	2011	19.85	19.87	20.01	20.2	19.7	18.61	17.54
	2012	22.24	22.26	21.79	21.96	22	22.19	21.77
	2013	25.07	24.72	25.07	25.24	25.49	26.47	23.25
	2014	29.78	30.40	30.75	30.28	30.72	31.57	27.03
	2015	38.08	37.74	37.74	38.48	37.33	37.66	32.42
	2016	47.09	46.93	45.85	47.55	45.83	44.91	42.94
	2017	54.48	54.95	55.25	56.19	55.28	53.57	50.55
	2018	64.4	63.81	65.22	65.69	65.02	63.9	57.6
	2019	75.84	76.27	74.79	77.51	75.42	76.21	69.75
	MAPE		0.81%	1.37%	1.48%	1.43%	2.67%	25.57%
Testing set	2020	79.35	87.07	82.66	94.86	86.87	77.69	80.31
	2021	87.98	88.19	92.34	110.08	96.25	93.03	79.39
	2022	89.81	89.79	101.13	128.68	104.64	111.39	78.49
	MAPE		3.33%	7.24%	29.32%	11.79%	10.62%	7.86%

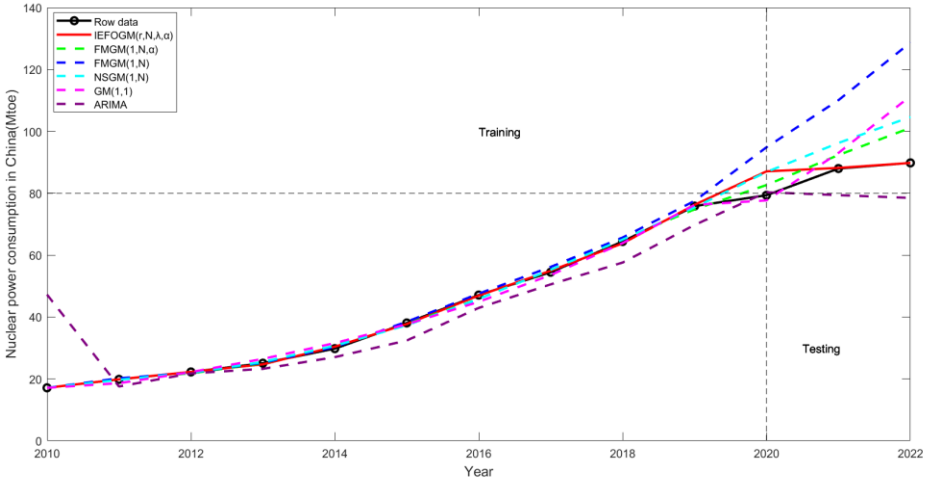

Figure 2. Comparison of fitted, predicted, and observed values for different models.

Based on the comparative analysis of multiple models, each model exhibits distinct fitting characteristics. The ARIMA model does not fit well on training sets and may not be able to capture the underlying patterns of the data very well. The GM(1,1) model demonstrates close alignment between the fitted values and the original data for certain years within the training set. However, on the test set, the MAPE reaches 10.62%, indicating insufficient stability in its performance on new data and weaker generalization capability. The NSGM(1,N) and FMGM(1,N) models demonstrated relatively stable performance on the training set, indicating good fitting capability, but there remains room for improvement in predictive accuracy. This substantial discrepancy between training and testing performance strongly suggests potential overfitting, which may lead to inadequate generalization when handling new data. The FMGM(1,N,α) model shows a satisfactory fitting performance in the training set. However, the outcomes on the testing set are still less than ideal, suggesting that the overall model fitting needs further improvement.

The IEFOGM(r,N,λ,α) model comprehensively considers linearity, nonlinearity, and interactions among driving factors, implementing multidimensional optimization. Among all models, the IEFOGM(r,N,λ,α) model demonstrated superior fitting performance. This fully demonstrates that the IEFOGM(r,N,λ,α) model exhibits strong adaptability to data characteristics while maintaining stable and accurate fitting capabilities across different data stages.

Case 2. China's carbon dioxide emissions prediction.

Scientific projections of CO_2 not only provide a scientific basis for the government to formulate emission reduction policies, optimize energy structures, and adjust industrial layouts, but also contribute significantly to global climate governance, demonstrating the responsibility of a major country. The modeling data in this study were selected from the carbon emission data and related factors of China in [35], as shown in Table 4. To validate the effectiveness of the IEFOGM(r,N,λ,α) model, we compared it with IEDGPM(1,N), IEGM(1,N), GPM(1,N), and GM(1,N) models. The fitting results of all models are presented in Table 5. Figure 3 visually contrasts the fitted curves from all comparative models against the original data sequence.

Table 4. Total CO_2 emissions and influencing factors.

Year	Total carbon emission (megaton)	Total energy consumption (Tons of standard coal)	Industrial structure (%)
2014	10,646	428,334	43.09
2015	10,548	434,113	40.84
2016	10,532	441,492	39.58
2017	10,767	455,827	39.85
2018	11,056	471,925	39.69
2019	11,311	487,488	38.59
2020	11,461	498,314	37.84
2021	12,040	524,000	39.43

Table 5. Modeling accuracy of different models.

	Year	Raw data	IEFOGM (r,N,λ,α)	IEDGPM (1,N)	IEGM (1,N)	GPM (1,N)	GM (1,N)
Training set	2014	10,646	10,646	10,646	10,646	10,646	10,646
	2015	10,548	10,552.99	10,490	8976	10,364	9065
	2016	10,532	10,535.22	10,539	11,404	10,666	11,466
	2017	10,767	10,770.95	10,674	10,994	10,944	11,049
	2018	11,056	11,059.03	10,942	11,073	11,059	11,128
	2019	11,311	11,309.78	11,211	11,310	11,113	11,282
	MAPE		0.03%	0.68%	5.09%	1.29%	5.29%
Testing set	2020	11,461	11,498.30	11,543	11,487	11,173	11,361
	2021	12,040	12,052.27	12,156	11,883	11,428	11,702
	MAPE		0.21%	0.84%	0.77%	3.80%	1.84%

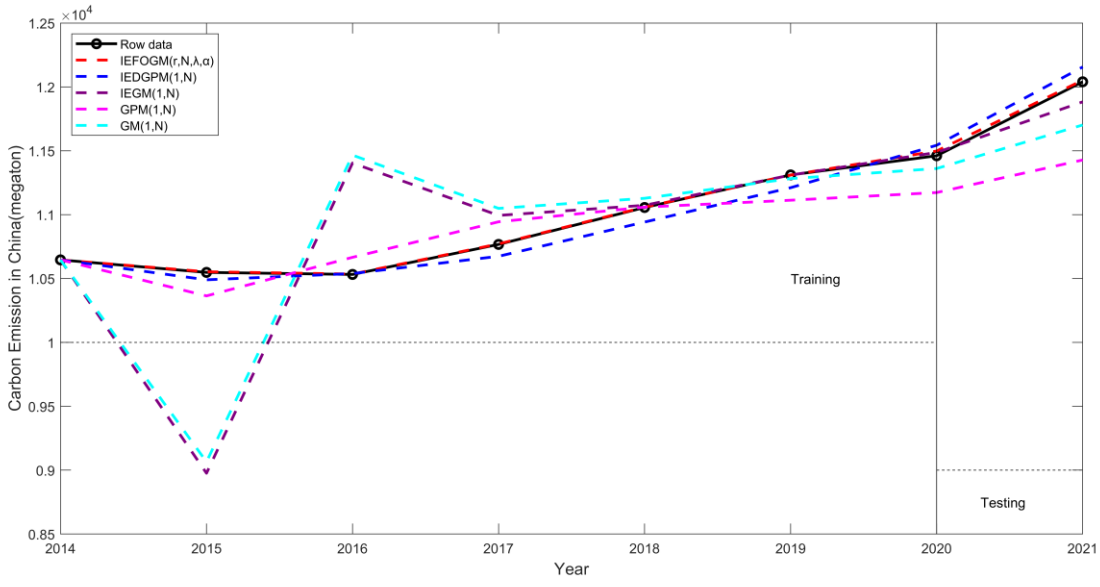

Figure 3. Model performance comparison.

As demonstrated in Table 5, each model exhibits distinct fitting characteristics. A MAPE of the IEDGPM(1,N) model achieves 0.68% on the training set, indicating that it is capable of effectively capturing the inherent patterns within the data. Although there is a slight increase in the value on the test set, it remains relatively low, indicating that the model maintains good performance on new data with strong generalization capability. The IEGM(1,N) and GM(1,N) models exhibit good predictive performance on the testing set, yet they show poor fitting accuracy on the training set. This indicates that the performance of these two models is insufficiently stable. The GPM(1,N) demonstrates satisfactory fitting capability, but its MAPE increases to 3.8% on the test set, indicating reduced predictive performance on new data and thus requiring improved generalization capability. In comparison, the IEFOGM(r,N,λ,α) model demonstrates remarkably outstanding fitting performance across both training and test sets, achieving MAPE values of 0.03% and 0.21%, respectively. Among all models evaluated, it exhibits exceptionally stable and highly accurate fitting capabilities at both training and testing sets. This strongly indicates that the IEFOGM(r,N,λ,α) model possesses superior data adaptability, maintaining extraordinary fitting consistency and precision across different data phases, thereby emerging as the most prominent performer among these models.

Case studies demonstrate that traditional models are often constrained when processing complex data features, whereas the IEFOGM(r,N,λ,α) model can dynamically adjust parameters to flexibly accommodate diverse types of data sequences. Building upon the NSGM(1,N) model, this model introduces multidimensional refinements and extensions, exhibiting exceptional performance in both adaptability and fitting accuracy. The application of dynamic background values enables adaptive adjustments based on the dynamic characteristics of data. The fractional-order accumulation significantly enhances the model's capability to characterize complex data features, thereby allowing the model to flexibly handle various types of data sequences. Furthermore, the proposed model fully considers the interactions among driving factors, effectively enhances the adaptability to complex multifactor coupling scenarios, and significantly broadens its application scope. The linear correction terms and nonlinear correction terms are precisely optimized for linear and nonlinear relationships. Through the synergistic effect of multifaceted optimizations, the fitting accuracy of the model is significantly enhanced, thereby providing more precise and reliable data support for the decision-making process.

4. Forecasting carbon dioxide emissions from energy consumption based on the IEFOGM(r,N,λ,α)

With the acceleration of global industrialization and rapid economic development, energy consumption continues to increase. The extensive utilization of fossil fuels emits substantial quantities of carbon dioxide. Under this context, accurately predicting CO_2 emissions from energy consumption holds crucial significance for developing scientific energy policies, optimizing energy structure, achieving emission reduction targets, and promoting sustainable development. The CO_2 emissions from energy consumption are influenced by multiple factors, including economic growth, technological innovation, fossil fuel consumption, industrial structure, policy regulations, and others [42]. The complexity and uncertainty inherent in these factors pose significant challenges to predicting CO_2 emissions from energy. To address this, this chapter will employ the IEFOGM(r,N,λ,α) model for predictive analysis of CO_2 emissions from energy consumption.

4.1. Identify relevant factors

4.1.1. Analysis of influencing factors

Considering the influencing factors and data availability, this paper selects R&D (Research and Experimental Development) intensity, energy processing and conversion efficiency, fossil energy consumption, and R&D expenditure as factors influencing CO_2 emissions from energy. Grey relational analysis is applied to identify the relevant factor sequences. The data on CO_2 emissions from energy consumption were sourced from the BP Statistical Review of World Energy. R&D intensity, energy processing and conversion efficiency, fossil energy consumption, and R&D expenditure were collected from the China Statistical Yearbook. Detailed numerical values are listed in Table 6.

Table 6. Carbon dioxide emissions from energy consumption and influencing factors.

Time	Carbon dioxide emissions from Energy (million tons)	Fossil energy consumption (ten thousand tons)	R&D intensity (%)	Energy processing and conversion efficiency (%)	R&D expenditure (hundred million yuan)
2011	8793.5	354,531	0.98	72.2	8687
2012	8977.6	363,131	1.2	72.7	10,298.4
2013	9214.1	374,388	1.26	73	11,846.6
2014	9235.5	379,932	1.33	73.1	13,015.6
2015	9171.3	382,019	1.43	73.4	14,169.9
2016	9014.6	384,098	1.53	73.5	15,676.7
2017	9270.3	393,835	1.61	73	17,606.1
2018	9610.7	403,496	1.93	72.8	19,677.9
2019	9933.7	412,902	2.27	73.3	22,143.6
2020	10,130.9	419,082	2.8	73.7	24,393.1
2021	10,563.5	438,071	2.43	73.2	27,956.3
2022	10,550.2	445,748	2.54	73.2	30,782.9

4.1.2. Correlation factor analysis

To thoroughly investigate the relationship between CO_2 emissions from energy consumption and their influencing factors, this study adopts Deng's grey relational degree (DGRD) to quantify the association between the comparative sequences and the system characteristic sequence (CO_2 emissions from energy consumption). The DGRD calculation formula is expressed as follows:

$$\gamma(x_0(k), x_i(k)) = \frac{\min_i \min_k | x_0(k) - x_i(k)| + \xi \max_i \max_k | x_0(k) - x_i(k)|}{| x_0(k) - x_i(k)| + \xi \max_i \max_k | x_0(k) - x_i(k)|}. \tag{36}$$

$$\gamma(X_0, X_i) = \frac{1}{n}\sum_{k=1}^{n}\gamma(x_0(k), x_i(k)). \tag{37}$$

The results calculated by Deng's grey relational degree are shown in Table 7.

Table 7. Results of correlation degree analysis.

Influencing factor	Correlation analysis result
R&D intensity	0.6648
Energy processing and conversion efficiency	0.9443
Fossil energy consumption	0.9737
R&D expenditure	0.6057

Based on the results of Deng's grey relational analysis, both the energy processing and conversion efficiency (X_2) and fossil energy consumption (X_3) exhibit relational degrees exceeding 0.9 with CO_2 emissions from energy consumption. In grey system theory, the relational degree above 0.9 indicates a strong correlation between factors. Therefore, X_2 and X_3 are selected as the correlated variables for the system behavior variable, i.e., carbon dioxide emissions from energy (X_1). X_2 and X_3 not only individually exert significant impacts on CO_2 emissions, but their interactive effects also impose comprehensive influences on CO_2 emissions. Energy processing and conversion efficiency affect the demand and consumption of fossil energy. We first hypothesize the existence of interactive effects between them and subsequently validate this hypothesis through an ablation experiment.

4.2. Modeling analysis

The model was established using the data from 2011 to 2019 as the training set, and the predictive performance was evaluated on the test set consisting of data from 2020 to 2022.

(1) Based on the objective function and constraints, dynamic optimization is performed using the genetic algorithm. When $r = 0.9312$, $\alpha = 5.7697$, and $\lambda = 0.7782$, the IEFOGM(r,N,λ,α) model achieves the minimum MAPE.

(2) Apply formula (13) to obtain the optimal parameter vector

$$\hat{p} = \left[0.0963, -26.5001, 6.4534, 1.3682, -0.0040, -21081.4049, 5223.8515\right]^T. \tag{38}$$

(3) By substituting the optimal parameters and parameter vector into formula (30), the time response sequence is obtained as

$$\begin{aligned}\hat{x}_1^{(0.9312)}(k) = \sum_{\nu=1}^{k-1}\Bigg\{0.4831\sum_{i=2}^{N}0.3374^{\nu-1}\Big[0.0963x_2^{(0.9312)}(k-\nu+1) - 26.5001x_3^{(0.9312)}(k-\nu+1) \\ +0.0006x_2^{(0.9312)}(k-\nu+1)x_3^{(0.9312)}(k-\nu+1)\Big]\Bigg\} + 0.3374^{k-1}\hat{x}_1^{(1)}(1) \\ +\sum_{u=2}^{k}(-0.0019)(0.3374)^{k-u}u^{5.7697} + \sum_{s=0}^{k-2}0.3374^{s}\left[-10210.0877(k-s)+2530.0013\right].\end{aligned} \tag{39}$$

For comparison, the HUGMC(1,N), FMGM(1,N,α), IEGM(1,N), NSGM(1,N), GM(1,N), GM(1,1), and ARIMA models were established to fit and predict CO_2 emissions from energy consumption. Detailed numerical outcomes are presented in Table 8.

According to the results presented in Table 8, the IEFOGM(r,N,λ,α) model achieves the highest fitting accuracy. Other prediction models not only exhibit larger errors compared to the IEFOGM(r,N,λ,α) model but also demonstrate larger fluctuation. The IEFOGM(r,N,λ,α) model maintains stability in both fitting and prediction phases, with a maximum error of 0.2292% and a minimum error as low as 0.0005%, significantly outperforming other models.

To more intuitively observe the performance of different models, we plotted a comparison graph using data from Table 8, as shown in Figure 4.

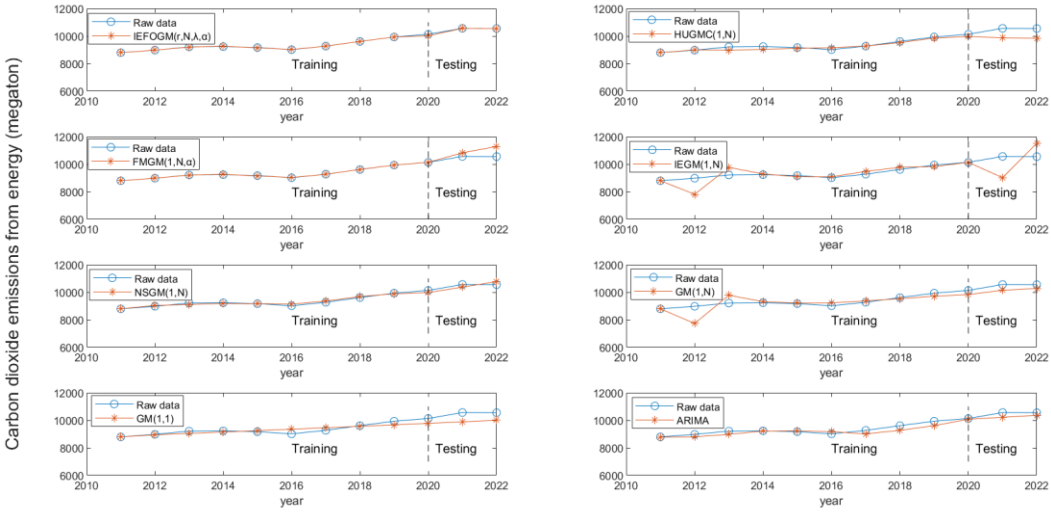

Figure 4. Comparison curves of different models.

As illustrated in Figure 4, the IEFOGM(r,N,λ,α) model demonstrates exceptional fitting performance, where the fitted value curve shows nearly perfect alignment with the original data curve. Through meticulous comparison of curve trends, we observe that the IEFOGM(r,N,λ,α) model not only precisely captures the rising and falling trends of original data but also maintains high consistency in the magnitude of numerical variations. However, the HUGMC(1,N), FMGM(1,N,α), IEGM(1,N), NSGM(1,N), GM(1,N), GM(1,1), and ARIMA models each have their limitations. The HUGMC(1,N) and FMGM(1,N,α) models demonstrate significant fluctuations in their predictions, making it difficult to capture the underlying trends in raw data. The NSGM(1,N) model demonstrates good fitting performance during the training set but shows noticeable deviations in test sets. The fitting accuracy of the IEGM(1,N) and GM(1,N) models for this dataset is not high, and some points exhibit significant fluctuations. While the GM(1,1) model can capture general trends, it remains insensitive to data fluctuations. The ARIMA model shows limited alignment with the original data in both training and test sets, with particularly large errors observed in certain years. Through comprehensive comparison, the IEFOGM(r,N,λ,α) model demonstrates the most superior performance.

To scientifically and rigorously evaluate the prediction accuracy of various models, three key metrics were selected: RMSE, MAE, and MAPE. A comparative analysis of errors across different models was conducted based on these indicators. Lower error values indicate higher model precision and more optimal modeling performance. Table 9 details the error of the comparative models and the IEFOGM(r,N,λ,α) model. Additionally, to visually observe the goodness of fit of each model, a comparative figure of error distributions is illustrated in Figure 5.

Table 8. Comparative analysis of models.

	Year	Raw data	IEFOGM(r,N,λ,α)	HUGMC(1,N)	FMGM(1,N,α)	IEGM(1,N)	NSGM(1,N)	GM(1,N)	GM(1,1)	ARIMA
Training set	2011	8793.5	8793.5	8793.5	8793.5	8793.5	8793.5	8793.5	8793.5	8784.7
	2012	8977.6	8980.56	8999.3	8978.54	7810.61	9038.18	7730.5	8943.71	8793.5
	2013	9214.1	9201.36	8966.97	9206.28	9763.62	9107.93	9779.5	9044.16	8977.6
	2014	9235.5	9256.67	9039.68	9255.86	9288.25	9181.59	9313.94	9145.74	9214.1
	2015	9171.3	9153.16	9106.17	9147.81	9087.58	9164.49	9210.2	9248.46	9235.5
	2016	9014.6	9024.61	9156.18	9029.12	9076.96	9135.78	9223.14	9352.34	9171.3
	2017	9270.3	9266.45	9274.56	9261.7	9470.07	9356.21	9370.11	9457.38	9014.6
	2018	9610.7	9610.65	9528.13	9616.74	9770.33	9687.87	9529.74	9563.6	9270.3
	2019	9933.7	9934.42	9856.31	9931.95	9822.58	9884.97	9709.93	9671.01	9610.7
	MAPE		0.0948%	1.1261%	0.1133%	3.2201%	0.7562%	3.4813%	1.6168%	1.8821%
Testing set	2020	10,131	10,023.92	9962.25	10,129.09	10,130.9	9974.05	9830.86	9779.64	10,076
	2021	10,564	10,558.54	9876.84	10,823.71	9017.55	10,372.31	10,142	9889.48	10,219
	2022	10,550	10,550.31	9844.12	11,278.72	11,518.18	10,771.37	10,274.9	10,000.6	10,361
	MAPE		0.3680%	4.9525%	3.1288%	8.2786%	1.8182%	3.1872%	5.0193%	1.8644%

Table 9. Precision comparison of different models.

	Error	IEFOGM (r,N,λ,α)	HUGMC (1,N)	FMGM (1,N,α)	IEGM(1,N)	NSGM(1,N)	GM(1,N)	GM(1,1)	ARIMA
Training set	MAPEtra	0.09%	1.13%	0.11%	3.22%	0.76%	3.48%	1.62%	1.88%
	MAEtra	8.705	104.4475	10.44	298.2325	70.0575	317.865	150.67	197.75
	RMSEtra	11.5317	130.8632	13.0032	468.409	77.693	449.0842	181.7726	224.8731
Testing set	MAPEtes	0.37%	4.95%	3.13%	8.28%	1.82%	3.19%	5.02%	1.86%
	MAEtes	37.35	520.4633	330.18	837.9767	189.7367	332.3	524.9767	196.1133
	RMSEtes	61.8313	576.9152	446.63	1053.0823	191.5478	338.3845	541.5415	229.1521

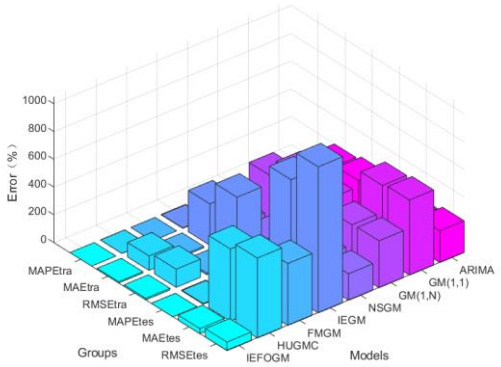

Figure 5. Model accuracy comparison diagram.

The column height of the IEFOGM(r,N,λ,α) model is significantly lower than that of other models under each error index. In terms of simulation error metrics, the IEFOGM(r,N,λ,α) model maintains errors at a lower level than traditional models. The performance gap becomes even more obvious in prediction error metrics, demonstrating its superior predictive accuracy in data forecasting.

4.3. Ablation experiment

Ablation experiments were conducted to demonstrate the necessity of each element in the IEFOGM(r,N,λ,α) model and to evaluate their impact on the overall performance. The model design for the ablation experiment is presented in Table 10. The results of the ablation experiment are specifically presented in Figure 6 and Table 11.

Table 10. Model design details for the ablation experiment.

Model	Ablation term	Interaction effects	Dynamic background value	Nonlinear corrections	Fractional-order accumulation
A	**b_{ij}=0**	×	√	√	√
B	**λ=0.5**	√	×	√	√
C	**α=0**	√	√	×	√
D	**r=1**	√	√	√	×
E	**r=1，b_{ij}=0**	×	√	√	×
F	**λ=0.5，b_{ij}=0**	×	×	√	√
G	**b_{ij}=0，r=1, λ=0.5，α=0**	×	×	×	×

As shown in the ablation experiment results in Table 11, when any of the interaction terms, dynamic background value, fractional-order accumulation, and nonlinear correction term in the model are ablated, all ablation models exhibit a significant decrease in model stability. This phenomenon fully demonstrates that each ablation term is crucial to the prediction accuracy and stability of the IEFOGM model: Removing interaction terms will cause the model to lose the ability to handle correlations between factors, and eliminating parameter optimization and model correction terms will significantly weaken its adaptability and stability. Experimental results confirm that model performance is strongly correlated with its components, and the absence of any key component may lead to a decline in comprehensive performance, thereby verifying the effectiveness of the IEFOGM model.

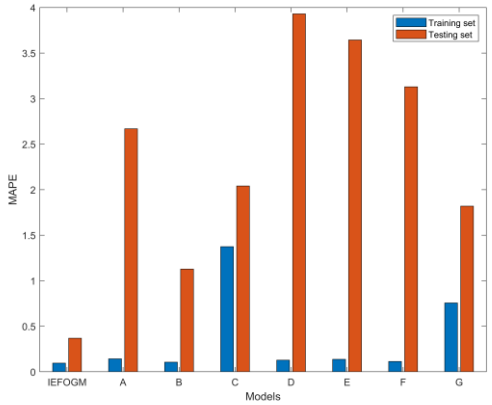

Figure 6. Comparison of MAPE distributions for the ablation experiment.

Table 11. Fitting and prediction results of the ablation experiment.

	Year	Raw data	IEFOGM	b_{ij}=0	λ=0.5	α=0	r=1	r=1, b_{ij}=0	λ=0.5, b_{ij}=0	b_{ij}=0，r=1, λ=0.5，α=0
Training	2011	8793.5	8793.5	8793.5	8793.5	8793.5	8793.5	8793.5	8793.5	8793.5
set	2012	8977.6	8980.56	8982.94	8980.88	8615.87	8983.46	8984.76	8978.54	9038.18
	2013	9214.1	9201.36	9194.68	9198.96	9186.03	9192.63	9189.96	9206.28	9107.93
	2014	9235.5	9256.67	9257.4	9259.27	9375.44	9263.8	9263.15	9255.86	9181.59
	2015	9171.3	9153.16	9158.93	9154.83	9306.38	9153.15	9157.4	9147.81	9164.49
	2016	9014.6	9024.61	9032.46	9018.44	9183.74	9025.47	9024.16	9029.12	9135.78
	2017	9270.3	9266.45	9249.74	9276.06	9373.27	9263.05	9259.39	9261.7	9356.21
	2018	9610.7	9610.65	9617.69	9603.19	9633.89	9612.18	9616.41	9616.74	9687.87
	2019	9933.7	9934.42	9933.72	9935.66	9889.78	9934.12	9932.26	9931.95	9884.97
		MAPE	0.0948%	0.1419%	0.1051%	1.3741%	0.1277%	0.1363%	0.1133%	0.7562%
Testing	2020	10,131.9	10,023.92	10,112.66	10,024.98	10,029.02	10,209.59	10,130.85	10,129.09	9974.05
set	2021	10,563.5	10,558.54	10,750.25	10,648.07	10,672.96	10,868.69	10,884.14	10,823.71	10,372.31
	2022	10,550.2	10,550.31	11,189.01	10,712.31	10,980.46	11,407.13	11,383.23	11,278.72	10,771.37
		MAPE	0.3680%	2.6676%	1.1276%	2.0400%	3.9294%	3.6439%	3.1288%	1.8182%

4.4. Prediction of carbon dioxide emissions from energy consumption

According to Table 8, the IEFOGM(r,N,λ,α) model demonstrates superior performance. Using simulation data from 2011 to 2019, the IEFOGM(r,N,λ,α) model was applied to predict carbon dioxide emissions from energy consumption for the next five years, with the prediction results summarized in Table 12.

Table 12. Prediction of carbon dioxide emissions from energy (million tons).

Year	2023	2024	2025	2026	2027
Prediction results	10,966.68	11,696.71	12,016.55	12,131.25	12,135.83

The results indicate that carbon dioxide emissions from energy consumption are projected to increase from 109.667 million tons in 2023 to 121.358 million tons in 2026. The growth rate of emissions is expected to slow down after 2025, demonstrating that current policies and technological measures have shown initial effectiveness in controlling emission growth. However, the overall trend remains upward. To achieve the carbon peaking target before 2030, it is imperative to phase down fossil fuels, accelerate energy transition, increase investments in renewable energy, and foster low-carbon innovation. Through comprehensive policy implementation, China can achieve green and low-carbon transformation while ensuring high-quality economic development, thereby making greater contributions to global climate governance. Although our projections indicate a deceleration in CO_2 emission growth from energy consumption in China, these emissions remain subject to multiple and complex influencing factors. To guarantee the smooth realization of the dual-carbon goals and sustainable development, relevant authorities must continue to strengthen monitoring and regulatory oversight.

5. Conclusions

In real social-economic systems, variables typically exhibit complex relationships, including linear, nonlinear, and interaction effects, which collectively influence system characteristics. To better capture these dynamics, we developed the IEFOGM(r,N,λ,α) model. By applying the IEFOGM(r,N,λ,α) model to the empirical study of carbon dioxide emissions from energy consumption in China, the following conclusions were drawn:

(1) The IEFOGM(r,N,λ,α) model, which is rooted in the NSGM(1,N) model, mitigates data randomness through fractional orders. It enhances the model's fitting precision by employing dynamic background values, integrates nonlinear correction terms to better capture the nonlinear characteristics, and introduces interaction terms to explain the effects of interactions on system characteristic variables, effectively addressing the modeling challenges of complex systems. This model adeptly captures subtle data pattern variations and demonstrates a remarkable capacity to extract data features and forecast trends.

(2) The IEFOGM(r,N,λ,α) model demonstrates strong adaptability and stability by dynamically adjusting parameters to flexibly handle different types of data sequences. When parameters vary, it achieves compatibility with eight traditional models, making it a robust tool applicable to diverse forecasting scenes.

(3) The case study results demonstrate that IEFOGM(r,N,λ,α) achieves exceptional accuracy in predicting China's CO_2 emissions from energy, with a training set error of merely 0.0948% and a testing set error of 0.3680%. Comparative validation against benchmark models confirms the superior simulation capability, predictive stability, and superiority of the IEFOGM(r,N,λ,α) model in

forecasting. By using the IEFOGM(r,N,λ,α) model to forecast China's CO_2 emissions from energy from 2023 to 2027, the results indicate that while emissions continue to rise overall, the growth rate is projected to slow down. To ensure the successful implementation of the carbon peaking target by 2030, it is imperative to accelerate the transition of the energy structure, reduce fossil fuel consumption, and achieve sustainable development.

(4) This study has focused simply on the interaction effect between two factors. When multiple relevant factors are involved, there may exist multifactor interaction effects, which should be more accurately characterized in future research to better delineate their impact on the system. In a real-world scene, policy implementation can exert significant influence on the system. Furthermore, time-delay effects between relevant factors and system behavior variables may exist. Incorporating delay effects could potentially enhance model precision by accounting for delayed responses in the system. We will strive to construct a better multivariate grey prediction model by considering factors such as interactions between multiple factors, dummy variables, and time lags, and by adopting new accumulation methods.

Author contributions

Shuangbing Guo: Conceptualization, writing- review and editing; Huanyu Zhou: Writing-original draft, methodology, formal analysis; Yuzhen Chen: Software, validation; Wenhao Gong: Investigation, data curation. All authors have read and approved the final version of the manuscript for publication.

Use of Generative-AI tools declaration

The authors declare they have not used Artificial Intelligence (AI) tools in the creation of this article.

Acknowledgments

This work was supported partly by the Key Scientific Research Projects of Colleges and Universities in Henan Province under Grant 24A110004, partly by Scientific and Technological Project in Henan Province of China under Grant 252102111064.

In the process of revising the paper, we sincerely thank the editor and all reviewers for their valuable time and energy in our article during this time. Because of your valuable comments, the quality of our articles has been qualitatively improved.

Conflict of interest

The authors declare that they have no conflicts of interest.

References

1. Y. Xiong, Energy problems and ecological civilization construction in China's industrialization, *Macroecon. Manage.*, **2** (2021), 51–58.
2. M. Z. Rehman, A. A. Dar, T. Wangmo A, Forecasting CO_2 emissions in India: A time series analysis using ARIMA, *Processes*, **12** (2024), 2699. https://doi.org/10.3390/pr12122699

3. M. C. Duan, Y. Duan, Prediction of energy consumption and carbon dioxide emissions in Gansu Province of China under the background of "Double Carbon", *Energies*, **17** (2024), 4842. https://doi.org/10.3390/en17194842
4. A. B. Ghorbal, A. Grine, I. Elbatal, E. M. Almetwally, M. M. Eid, E. S. M. E. Kenawy, Predicting carbon dioxide emissions using deep learning and Ninja metaheuristic optimization algorithm, *Sci. Rep.*, **15** (2025), 4021. https://doi.org/10.1038/s41598-025-86251-0
5. H. Moayedi, A. Mukhtar, B. N. Khedher, N. Khalilpoor, H. Moayedi, A. Mukhtar, et al., Forecasting of energy-related carbon dioxide emission using ANN combined with hybrid metaheuristic optimization algorithms, *Eng. Appl. Comp. Fluid*, **18** (2024), 2322509. https://doi.org/10.1080/19942060.2024.2322509
6. J. L. Deng, Control problems of grey systems, *Syst. Control Lett.*, **1** (1982), 288–294.
7. J. Jiang, Y. Ban, S. Nong, Novel discrete grey Bernoulli seasonal model with a time powter term for predicting monthly carbon dioxide emissions in the United States, *Front. Env. Sci.*, **12** (2025), 1513387. https://doi.org/10.3389/fenvs.2024.1513387
8. Z. R. Qiao, X. M. Meng, L. F. Wu, Forecasting carbon dioxide emissions in APEC member countries by a new cumulative grey model, *Ecol. Indic.*, **125** (2021), 107593. https://doi.org/10.1016/j.ecolind.2021.107593
9. W. Y. Qian, Y. G. Dang, Y. M. Wang, Weighted accumulation generation-based GM(1,1) model and its application, *Math. Pract. Theory*, **39** (2015), 47–51.
10. S. F. Liu, *Grey system theory and its application*, 9 Eds, Beijing: Science Press, 2021.
11. F. Qin, M. Tong, Y. Huang, Y. Zhang, Modeling, prediction and analysis of natural gas consumption in China using a novel dynamic nonlinear multivariable grey delay model, *Energy*, **305** (2024), 132105. https://doi.org/10.1016/j.energy.2024.132105
12. Z. Hu, T. Jiang, Innovative grey multivariate prediction model for forecasting Chinese natural gas consumption, *Alex. Eng. J.*, **103** (2024), 384–392. https://doi.org/10.1016/j.aej.2024.06.012
13. B. Zeng, H. Li, X. Ma, A novel multi-variable grey forecasting model and its application in forecasting the grain production in China, *Comput. Ind. Eng.*, **150** (2025), 106915. https://doi.org/10.1016/j.cie.2020.106915
14. W. Yang, Z. Qiao, L. Wu, X. Ren, F. T. Hesary, Forecasting carbon dioxide emissions using adjacent accumulation multivariable grey model, *Gondwana Res.*, **134** (2024), 107–122. https://doi.org/10.1016/j.gr.2024.06.015
15. L. Zhang, X. Ma, A novel multi-fractional multivariate grey model for city air quality index prediction in China, *Expert Syst. Appl.*, **257** (2024), 125010. https://doi.org/10.1016/j.eswa.2024.125010
16. D. Luo, B. Wei, Grey forecasting model with polynomial term and its optimization, *J. Grey Syst.*, **29** (2017), 58–69.
17. Y. G. Dang, S. F. Liu, K. J. Chen, The GM models that x (n) be taken as initial value, *Kybernetes*, **33** (2004), 247–254.
18. B. Liu, S. F. Liu, Z. J. Zhai, Y. G. Dang, Optimization of the time response function in the GM(1,1) model, *Chinese J. Manage. Sci.*, **4** (2003), 55–58. https://doi.org/10.16381/j.cnki.issn1003-207x.2003.04.011
19. L. F. Wu, S. F. Liu, L. G. Yao, S. L. Yan, D. L. Liu, Grey system model with the fractional order accumulation, *Commun. Nonlinear Sci.*, **18** (2013), 1775–1785. https://doi.org/10.1016/j.cnsns.2012.11.017
20. X. K. Yu, S. H. Mao, Y. H. Zhang, Variable order fractional grey model and its application, *Appl. Math. Model.*, **97** (2021), 619–635. https://doi.org/10.1016/j.apm.2021.03.059

21. B. Zeng, T. Zheng, Y. Yang, J. Wang, A novel grey Verhulst model with four parameters and its application to forecast the carbon dioxide emissions in China, *Sci. Total Environ.*, **899** (2023), 165648. https://doi.org/10.1016/j.scitotenv.2023.165648
22. Y. Z. Chen, W. H. Gong, S. Z. Li, S. B. Guo, A novel conformable fractional-order accumulation grey model and its applications in forecasting energy consumption of China, *Sci. Rep.*, **14** (2024), 31028. https://doi.org/10.1038/s41598-024-82128-w
23. Y. Wang, Z. Yang, Y. Luo, R. Yang, L. Sun, F. E. Sapnken, et al., A novel structural adaptive Caputo fractional order derivative multivariate grey model and its application in China's energy production and consumption prediction, *Energy*, **312** (2024), 133622. https://doi.org/10.1016/j.energy.2024.133622
24. B. Zeng, C. Li, Improved multi-variable grey forecasting model with a dynamic background-value coefficient and its application, *Comput. Ind. Eng.*, **118** (2018), 278–290. https://doi.org/10.1016/j.cie.2018.02.042
25. H. L. Huang, Z. F. Tao, J. P. Liu, J. H. Cheng, H. Y. Chen, Exploiting fractional accumulation and background value optimization in multivariate interval grey prediction model and its application, *Eng. Appl. Artif. Intel.*, **104** (2021), 104360. https://doi.org/10.1016/j.engappai.2021.104360
26. N. Xie, S. Liu, Discrete grey forecasting model and its optimization, *Appl. Math. Model.*, **33** (2008), 1173–1186. https://doi.org/10.1016/j.apm.2008.01.011
27. X. Ma, Z. B. Liu, Predicting the oil field production using the novel discrete GM(1,N) model, *J. Grey Syst.*, **27** (2015), 63–73.
28. S. Ding, Y. G. Dang, N. Xu, Construction and application of GM(1, N) model based on dummy variable control, *Control Decision*, **33** (2018), 309–314. https://doi.org/10.13195/j.kzyjc.2016.1613
29. Z. X. Wang, Multivariate GM(1,N) model with interactive effects, *Control Decision*, **32** (2017), 515–520. https://doi.org/10.13195/j.kzyjc.2016.0138
30. S. Ding, Y. Dang, L. Xu, J. Wang, Multivariable grey forecasting model based on interaction effect and its application, *Syst. Eng. Electron.*, **40** (2018), 595–602. http://dx.doi.org/10.3969/j.issn.1001-506X.2018.03.17
31. H. M. Duan, X. Y. Pang, A novel grey prediction model with system structure based on energy background: A case study of Chinese electricity, *J. Clean. Prod.*, **390** (2023), 595–602. https://doi.org/10.1016/j.jclepro.2023.136099
32. L. Xia, Y. Ren, Y. Wang, Y. Fu, A novel dynamic structural adaptive multivariable grey model and its application in China's solar energy generation forecasting, *Energy*, **312** (2014), 133534. https://doi.org/10.1016/j.energy.2024.133534
33. C. Li, Y. Li. J. Xing, Multivariate grey prediction model application in civil aviation carbon emission based on fractional order accumulation and background value optimization, *Sustainability*, **15** (2023), 9127. https://doi.org/10.3390/su15119127
34. B. Zeng, H. Duan, Y. Zhou, A new multivariable grey prediction model with structure compatibility, *Appl. Math. Model.*, **75** (2019), 385–397. https://doi.org/10.1016/j.apm.2019.05.044
35. Q. Si, *Construction of a time-delay GM(1,N) power model considering interaction effects and its application in carbon emission prediction*, Master's Thesis, Wuxi: Jiangnan University, 2022.
36. Y. T. Li, *Research on multivariable heterogeneous accumulation grey prediction model and its application*, Master's Thesis, Handan: Hebei University of Engineering, 2024.
37. B. Zeng, S. L. Li, W. Meng, *Grey prediction theory and its applications*, 1 Ed, Beijing: Science Press, 2020.
38. W. Meng, Research on fractional-order grey reducing generation operator and its properties, *Math. Pract. Theory*, **50** (2020), 192–197. http://dx.doi.org/10.1109/gsis.2015.7301824

39. B. Zeng, W. Meng, M. Tong, A self-adaptive intelligence grey predictive model with alterable structure and its application, *Eng. Appl. Artif. Intel.*, **50** (2016), 236–244. https://doi.org/10.1016/j.engappai.2015.12.011
40. H. T. Ren, *Optimization of two types of multivariable grey prediction models*, Master's Thesis, Zhengzhou: Henan Agricultural University, 2024.
41. S. Ding, Y. Dang, L. Xu, J. Wang, Multivariable grey forecasting model based on interaction effect and its application, *Syst. Eng. Electron.*, **40** (2018), 595–602. http://dx.doi.org/10.3969/j.issn.1001-506X.2018.03.17
42. F. M. Mirza, A. Sinha, J. R. Khan, O. A. Kalugina, M. W. Zafar, Impact of energy efficiency on CO2 Emissions: Empirical evidence from developing countries, *Gondwana Res.*, **106** (2022), 64–77. https://doi.org/10.1016/j.gr.2021.11.017

AIMS Press